 doi:10.20944/preprints201808.0046.v1

Hexagonal β-$Co(OH)_2$ nanoparticle as a precursor in a solution-processed $LiCoO_2$ and its electrochemical properties

R. Samal[a,b], P. P. Dahiya[c], S. B. Majumder[c], B. Dash[a,*], K. Sanjay[a], M. Barmi[d], and M. Minakshi[d]

[a] *CSIR- Institute of Minerals and Materials Technology, Bhubaneswar 751013,* ***India***
[b] *Academy of Scientific and Innovative Research (AcSIR), Training and Development Complex, CSIR Road, Taramani, Chennai 600113,* ***India***
[c] *Materials Science Centre, Indian Institute of Technology, Kharagpur-721302,* ***India***
[d] *Engineering and Information Technology, Murdoch University, WA 6150,* ***Australia***

Abstract

Crystalline β-cobalt hydroxide (β-$Co(OH)_2$) of different morphologies have been successfully synthesized with the addition of sodium hydroxide to cobalt nitrate solution and aging in the mother liquor. The rate of NaOH addition, ranging from 0.1 mL/min to 10 mL/min, influences the surface morphology with the obtained storage capability of the respective electrode. Characterization of the β-$Co(OH)_2$ was fully developed, including X-ray diffraction, scanning and transmission electron microscopy, and BET analyses. At a lower rate of NaOH addition, particles are like platelets, while for a higher rate (≥ 2 mL/min) grains are fused together forming a larger crystallite size. This result is supported by the X-ray diffraction structural analysis, where the phase evolution of (002) plane becomes distinct for the higher rate of NaOH addition. Lithium cobalt oxide ($LiCoO_2$) was synthesized through oxidation from the as-prepared β-$Co(OH)_2$ and LiOH. The electrochemical performance of as obtained $LiCoO_2$ is investigated using charge-discharge and cyclic voltammetric studies. The precursor β-$Co(OH)_2$ prepared at a lower rate of 0.1 mL/min in $LiCoO_2$ demonstrated the best electrochemical performance of 155 mAh/g. After 50 cycles, the capacity retention rate was 67% compared with the first cycle. Finally, we have attempted to correlate the amount of the available OH^- ions with the formation of platelets and the discharge capacity. This work has developed a methodology for the synthesis of $LiCoO_2$ using β-$Co(OH)_2$ in a facile chemical solution process.

Keywords: *Cobalt hydroxide, $LiCoO_2$, Lithium-ion battery*

Email: Barsha.dash@gmail.com (Barsha Dash); minakshi@murdoch.edu.au (M. Minakshi)

Preprints (www.preprints.org) | NOT PEER-REVIEWED | Posted: 2 August 2018 doi:10.20944/preprints201808.0046.v1

Introduction

Currently, fossil fuels play a major role in the total world primary energy consumption, but the main issues associated with the fossil fuels are finite resources and produces significant CO_2 emissions into the atmosphere. Therefore, alternative source of energy (such as from renewable resources) will be part of the energy economy in the future. As the renewable energy resources are intermittent, the demand for reliable batteries is rising, so that the excess energy can be stored and used it later [1]. Rechargeable batteries are devices which can store and release electric energy repeatedly. The lithium-ion battery has significantly higher energy density and power density (at least 2 – 3 times) than lead-acid, Ni-Cd, and Ni-MH batteries [2]. Li-ion battery has found a wide range of applications, ranging from portable electronics, power tools, to electric vehicles (EVs). However, the development of this battery requires extensive research on cathode materials [3]. Lithium cobalt oxide ($LiCoO_2$) remains as one of the most attractive positive electrode materials that has received much attention for lithium secondary batteries [4-5].

$LiCoO_2$ having a layered structure [6], composed of a closed-packed network of oxygen, is used as a cathode for high-energy systems [7, 8] which has the structural limitation of the capacity >140 mAh g^{-1} at a potential >3.4 V vs. Li/Li^+. The extraction of Li from $LiCoO_2$ beyond 0.5 Li is limited, means $LiCoO_2$ can only deliver half of its theoretical capacity of 247 mAh g^{-1}. Early studies on $LiCoO_2$ have demonstrated the well-developed synthetic routes that can enhance specific capacity through doping with trivalent ions and coating with metal oxides, and the ability for facile synthesis for mass production [4, 9]. However, the toxicity and high cost of additives limited the use of applying a coating or incorporating the additives in $LiCoO_2$. Alternatively, there is a number of other ways to enhance the performance, such as, synthesize $LiCoO_2$ from its

Preprints (www.preprints.org) | NOT PEER-REVIEWED | Posted: 2 August 2018 doi:10.20944/preprints201808.0046.v1

well-known precursor cobalt hydroxide/oxide [10–13] using methods such as sol-gel [14], spray-drying [15], and rotary evaporation method [16]. Recently, there were few reports on using both cobalt hydroxides such as $Co(OH)_2$ and α-$Co(OH)_2$ as negative electrodes for battery applications [17-18]. However, the tailored β-$Co(OH)_2$ nanoparticle as a precursor to synthesize $LiCoO_2$ and testing its suitability as a cathode for battery studies in non-aqueous solvents has not been reported.

Cobalt oxyhydroxide, $Co(OH)_2$, has been reported to crystallize in two different forms, α and β, with layered hexagonal crystal structures [19]. The α-form is isostructural with hydrotalcite-like structure, which is inclined to losing interlayer water and become metastable. While the β-form is brucite-like structure and consists of a hexagonal packing of hydroxyl ions with Co (II) occupying alternative rows of octahedral sites without any intercalation process into an interlayer space. Therefore, a β form of $Co(OH)_2$ is expected to be more promising than their counterpart, α form [20]. The objectives of the current work are (a) to controllably synthesize a series of β-$Co(OH)_2$ nanoparticles with different morphologies while varying the rate of addition of the reagent (NaOH). (b) to use the β-$Co(OH)_2$ as precursor mixed along with LiOH to synthesize $LiCoO_2$ by a simple chemical solution process, (c) then to investigate their electrochemical properties for potential energy storage (battery) applications.

Experimental

The reagents $Co(NO_3)_2.6H_2O$, NaOH, Nitric acid, and LiOH used were analytical grade purchased from Merck Chem. Ltd., India.

Synthesis

In a typical synthesis of β-$Co(OH)_2$ nanoparticles: 1M NaOH solution was added dropwise into the beaker containing cobalt nitrate solution while varying the rate of

Preprints (www.preprints.org) | NOT PEER-REVIEWED | Posted: 2 August 2018 doi:10.20944/preprints201808.0046.v1

addition of the NaOH ranging from 0.1, 1, 2, 5 and 10 mL/min. The deposition of cobalt hydroxide was carried out by controlling the pH of the mother liquor of the solution from pH 4 to 8.5. After precipitation, the as-obtained product was filtered followed by washing in de-ionized water until the pH of filtrate attains a value ~7. Then the filtrate was further washed with ethanol followed by drying at 80°C.

In a typical synthesis of $LiCoO_2$: the Stoichiometric amount of as synthesized β-$Co(OH)_2$ is mixed with lithium hydroxide (LiOH) and heated in a furnace at 450ºC for 3 h in air. Then, it was furnace cooled and the resultant powder was mixed with the binder, polyvinyl alcohol (PVA), in order to make a pellet. Finally, the samples in a pellet form were sintered at 850ºC for 10 h in air. The final product is $LiCoO_2$ in a single phase without any impurities.

Physical Characterization

An X-ray diffractometer (PANalytical PW 1830; Philips, Japan) with Mo-Kα radiation (λ =0.70932A°) was used to determine the preferred crystal orientation and phase purity of the deposited cobalt hydroxide, $Co(OH)_2$. The deposits were also analysed by scanning electron microscope (SEM, JEOL JSM 6510, Japan) to view the morphology of the Cobalt hydroxide prepared under various deposition conditions. Transmission Electron Microscope (FEI, TECNAI G2 20, TWIN, (FEI (Philips), Almelo, The Netherlands) operated at 200 kV was used to study the internal features of the synthesized $Co(OH)_2$ samples. For TEM analysis, a very dilute suspension of the sample was put on carbon-coated Cu grids after dispersing in acetone medium.

Electrochemical characterization

Electrochemical experiments were carried out via coin cell (2025 type coin cell). To prepare the cathode, as-prepared materials $LiCoO_2$ derived from ($Co(OH)_2$) mixed with acetylene black, and polyvinylidene fluoride (PVDF) binder in a weight ratio of 80:10:10

Preprints (www.preprints.org) | NOT PEER-REVIEWED | Posted: 2 August 2018 doi:10.20944/preprints201808.0046.v1

was dispersed in a N-methyl-2-pyrrolidone (NMP) solution to make a slurry. The mixed slurry was coated on a copper Al foil and dried in a vacuum oven at 90ºC overnight prior to coin-cell assembly. The cells were assembled in a glove box (Mbraun, Germany) filled with ultrahigh purity argon with metallic Li anode, polypropylene membrane as the separator, and a 1M $LiPF_6$ in ethylene carbonate/dimethyl carbonate (EC/DMC) (1:1 v/v) as the electrolyte. Galvanostatic charge/discharge and cycling test were evaluated using a Land Battery Tester (Land CT 2001A, Wuhan, China) within the voltage range of 3 V – 4.5 V (vs. Li/Li^+) at room temperature.

Results and Discussion

I. Structural analysis

X-ray diffraction (XRD)

The XRD patterns of the as-synthesized product are presented in Fig. 1. All the diffraction peaks can be ascribed to the pure brucite-like crystal structure of β-$Co(OH)_2$ (adopting a hexagonal structure and the pattern is in good agreement with those reported in the literature JCPDS card 00-001-0357) [21-22]. The XRD patterns of all the samples obtained by varying the rate of NaOH addition is characterized by the Bragg reflection intensity of the doublet, (101) and (002) peaks. The inset in Fig. 1, clearly shows the variation in the intensity of the doublet indicating that the preferential orientation was changed from (101) to (002), which could be a reason for varied surface morphology (detailed in the next section; SEM). For the slowest rate i.e. 0.1 mL/min, weak Bragg reflection is observed for (002) plane, while the reflection for (101) plane is strong. Interestingly, with the increase in the rate of NaOH addition, the (002) peak grows gradually and the intensities of the (101) and (002) peaks become equal at the rate of 1 mL/min. From thereon, (002) peak supersedes and becomes dominant. With reference to the standard JCPDS pattern and work reported earlier [21], an

Preprints (www.preprints.org) | NOT PEER-REVIEWED | Posted: 2 August 2018 doi:10.20944/preprints201808.0046.v1

intensity of the (002) peak is not strong, as opposed to the strong peak observed in this work in Fig. 1. This unusual observation could be due to the fact that OH^- ions are absorbed onto the cobalt hydroxide (002) plane, and resulted in a preferential orientation on the sample surface. From the crystallographic point, it can be explained in a way that (101) plane has only one growing site in the b-axis, whereas in the case of (002) plane, there are two growing sites in both a and b axes. Hartman et al [23] described the specific compound have a variety of morphology based on the crystal planes. Therefore, the sizes of the platelets like crystals are expected to be bigger with the rate of NaOH addition but only to an extent of 2 mL/min. At a higher rate (≥ 2 mL/min) the tendency of the crystal formation is fused towards the formation of a nucleus, however, the particle size is still in nano size. As shown in Fig. 2a when the rate of OH^- ion addition is very slow, the cobalt ion is surrounded by very few OH^- ion. This is to say the number of OH^- per cobalt ion was just adequate. The case is opposed to the higher rate (Fig. 2b), and this could explain the evolution of (002) peak through variation of the concentration of NaOH at a fixed cobalt nitrate concentration. After the optimized value of 2 mL/min, the population of OH^- ion becomes too high [24] in the vicinity of each cobalt ion, as illustrated in the diagram Fig. 2b, thus the grains fused together forming small crystals (detailed in the next section; SEM). Obviously, the rate of NaOH addition influences the pH of the solution, the crystallite size of β-$Co(OH)_2$ and the phase evolution of (002) peak support this fact profoundly.

SEM and TEM studies

The morphology and texture of the as-synthesized β-$Co(OH)_2$ samples prepared at the different rate of NaOH addition have been studied through SEM and presented in Fig. 3. The surface morphology was changed by increasing the concentration of NaOH, the observed trend is quite similar to those reported in the literature but for the material ZnO [24]. The

Preprints (www.preprints.org) | NOT PEER-REVIEWED | Posted: 2 August 2018 doi:10.20944/preprints201808.0046.v1

observed initial irregular morphologies (Fig. 3a-b) are due to low pH in the solution (scarce of OH^- ions). In Fig. 3 c-f, the SEM images reveal that the particles got more flattened with the addition of the NaOH from 0.5 mL/min to 2 mL/ min. A similar sort of morphology reported for this material [23, 25] displaying a platelet-like shape indicates the formation of cobalt oxyhydroxide. At ≥ 2 mL/min, the excess OH^- ions in the vicinity of cobalt ions were absorbed onto the cobalt surface. As a result, as-synthesized β-$Co(OH)_2$ particles appears to take a different shape of tiny clusters (Fig. 3g-h). At a higher magnification, the clusters are more visible suggesting that newly-formed nuclei agglomerated to form bigger secondary particles resulting in clusters.

To gain more insight into the internal features of the obtained product, transmission electron microscopy was conducted and the corresponding images were shown in Fig. 4. TEM images revealed that the structure of as-prepared β-$Co(OH)_2$ is a typical hexagonal structured nanoplatelet as evidenced from Fig. 4a. The length of the nanoparticle, calculated using Image J software, is found to be in the range of 20-25 nm. Fig 4b depicts that though the β-$Co(OH)_2$ is invariably shown to be hexagonal in shape, the particle sizes varies significantly. The selected area diffraction pattern of the particles shown in Fig. 4c shows a series of Debye rings with bright spots illustrating that he particles are crystalline in nature, supporting the diffraction pattern observed in Fig. 1. The inter-planar distance between two lattice fringes was evaluated as 0.244 nm (Fig. 4d), which is in excellent agreement with the (101) crystal plane.

Particle size analysis

The particle size and morphology of solution-processed β-$Co(OH)_2$ is shown to be controlled by concentrations of the NaOH addition that influences the particle nucleation and growth mechanisms. Table 1 gives an overview of particle size obtained from the product at various

Preprints (www.preprints.org) | NOT PEER-REVIEWED | Posted: 2 August 2018 doi:10.20944/preprints201808.0046.v1

solution concentrations. The particle size distribution reveals a similar trend to that of XRD and SEM that the particle size increases until the rate of NaOH addition reaches an optimum value and then it started to reduce. Table 1 shows that for 0.1 mL/min the particle size is 237 nm for 50 % (otherwise termed as D_{50}) of particles and 290 nm for 90% (D_{90}) of particles. The D_{50} is the "mass median diameter" as it divides the sample equally by mass. However, with the concentration of 2 mL/min, the particle size further increases to 525 nm for 50% particles and 2939 nm for 90% particles. At ≥ 2 mL/min, sizes reduced to 232 nm for 50% particles and 973 nm for 90% particles for 5 mL/min and finally it dropped to 539 nm for 90% particles with 10 mL/min rate of addition.

FTIR analysis

FT-IR spectra of the as-synthesized β-$Co(OH)_2$ samples prepared at the different rate of NaOH addition are shown in Fig. 5. Several absorption peaks are evidenced and the peak numbers are labeled in the respective spectra. For the lower concentration, 0.1 mL/min, three absorption peaks were identified in the mid-frequency region. The peak at 591 cm^{-1} is assigned to C-Br stretching (m) vibration. The band at 659 cm^{-1} corresponds to the σ O–H wagging vibration. The peak at 1384 cm^{-1} is related to the ν3 vibrational modes of NO_3^- intercalated in the interlayers [20, 26]. For 1, 5 and 10 mL/min samples, an evolution of new absorption peaks were observed. IR peaks at 1083 cm^{-1} and 1033 cm^{-1} are assigned to the C-N stretching (m) vibration. In case of 1 mL/ min, an additional peak appears at the position of 795 cm^{-1} may be attributed to C-Cl stretching (m) vibration. A peak at 1631 cm^{-1} for 50 and 100 mL/min is due to N-H bending vibration. The band at all the high wavenumbers, for the samples analyzed, can be assigned to the stretching vibration of hydroxyl group [21]. The peaks at 3428 cm^{-1} and 3441 cm^{-1} and 3435 cm^{-1} may be attributed to H^- bonded -OH stretching vibration for 0.1, 1, and 10 mL/min, respectively. The presence of excess OH^- ions on the surface of the β-$Co(OH)_2$ is evidenced by the infra-red analysis.

Preprints (www.preprints.org) | NOT PEER-REVIEWED | Posted: 2 August 2018 doi:10.20944/preprints201808.0046.v1

II. Electrochemical analysis

Charge-discharge and cyclic voltammetric analyses

The use of transition metal oxides such as $LiCoO_2$ as the positive electrode has been widely studied for Li-ion rechargeable batteries. The achievable capacity of $LiCoO_2$ is reported to be 147 mAh g^{-1} based on the 0.5 extraction of Li ions from this cathode material [3-4]. The electrochemical activity of the $LiCoO_2$ prepared from the as obtained β-$Co(OH)_2$ as a precursor mixed with LiOH was tested through multiple charge-discharge analysis. Fig. 6a shows a typical voltage vs. capacity profile for $LiCoO_2$ prepared at a rate of 0.1 mL/min. The corresponding dQ/dV plot is presented in Fig. 6b. The process is fully reversible with a flat discharge mid-potential of 4 V before it falls sharply down to the cut-off voltage 3 V. The first discharge capacity is found to be ~155 mAh/g when cycled at C/10 current rate. The discharge/charge mechanism could correspond to a facile intercalation/extraction of lithium ions into/from the layered structure of lithium cobalt oxide. The Li^+ intercalation leads to the reduction of Co^{4+} ions into Co^{3+} and in the subsequent charge, Co^{3+} ions are oxidized back to Co^{4+} oxidation state [3-4]. The redox process of cobalt ions (+3/+4) is known to take place at ~4.0V with respect to Li^+/Li. The phenomenon is clearly visible in the dQ/dV plot presented in Fig. 6b. As shown in Fig. 6b, the oxidation takes place ~4.1V during the first charge and the corresponding reduction can be observed at ~3.9 V during discharge. In the subsequent cycle of charge, the oxidation is slightly shifted to lower potential value, whereas the reduction takes place at the same potential. All the $LiCoO_2$ samples were found to be electrochemically active in delivering multiple intercalation/de-intercalation of Li^+ ions into the structure. The charge-discharge profiles for 2 mL/min and 10 mL/min showed a similar shape of curves (not shown here) but with a slightly a meager in available capacities, such as 150 mAh g^{-1} and 145 mAh g^{-1}, respectively. However, in terms of cyclability, a significant difference has been observed.

Preprints (www.preprints.org) | NOT PEER-REVIEWED | Posted: 2 August 2018 doi:10.20944/preprints201808.0046.v1

The cyclability performance measured at C/10 current rate for the $LiCoO_2$ samples prepared by varying rate of NaOH is presented in Fig. 7. The highest discharge capacity ~155mAh/g was obtained for the sample prepared at the slowest NaOH addition rate 0.1 mL/min. To be noted, $LiCoO_2$ prepared from the high rate of NaOH addition (10 mL/min) showed (Fig. 7) a dramatic drop in the 2^{nd} cycle. This could be due to the structural instability and excessive reaction of OH^- particles with an electrolyte which leads to the formation of unfavorable by-products. The samples prepared with the relatively lower rate of reagent addition (0.1 mL/min and 2 mL/min) do not show such anomaly. The reason may be attributed to the fact that with the slow availability of the OH^- ion, the crystals would have developed more homogenously as compared to the samples with the high rate of addition. Table 2 summarizes the discharge capacity at various cycles until 50 % capacity retention after 50 cycles of charge/discharge at C/10 discharge current, and average capacity fading rate for $LiCoO_2$ prepared at various rates of reagent addition.

The sample prepared at slowest addition rate is found to be good at delivering better cyclability and capacity retention as compared to the samples prepared at relatively higher addition rate (10 mL/min). If we analyse the average capacity loss per cycle, the loss is comparable for 0.1 mL/min and 2 mL/min whereas for 10 mL/min there is a drastic rise in the loss per cycle (4.6) as shown in Table 2. This loss is mainly observed from the second cycle onwards. This behaviour proves the presence of imperfection in crystallization of sample prepared at a high rate of NaOH addition. Thus enhanced electrochemical performance was revealed by the slow addition of reagent that influences the morphology and correlates the structural and electrochemical properties.

Preprints (www.preprints.org) | NOT PEER-REVIEWED | Posted: 2 August 2018 doi:10.20944/preprints201808.0046.v1

Conclusions

Chemical deposition of cobalt hydroxide was carried out in cobalt nitrate with the addition of NaOH at varying rates ranging from 0.1 mL/min to 10 mL/min. The $Co(OH)_2$ was identified as the β form with a brucite-like structure. At a higher rate (≥ 2 mL/min) of NaOH in the solution, a larger amount of OH^- ions deposits on the sample surface in the (002) plane and the particles are found to fused together with a lower particle size. The as-synthesized β-$Co(OH)_2$ with an optimum rate of NaOH addition chosen as a precursor for $LiCoO_2$ was tested for its suitability as a cathode material in Li-ion battery as cathode. The $LiCoO_2$ showed a discharge capacity of 155 mAh/g. After 40 cycles, the capacity had decreased by less than 2% compared with the first cycle. These results confirmed the potential application of the prepared β-$Co(OH)_2$ nanoparticles with a platelet shape as a suitable precursor for a battery electrode $LiCoO_2$.

Acknowledgment

The authors are thankful to Director, CSIR-IMMT for proving all the facility to carry out research work. The authors are also thankful to MoES for financial support.

References

1. A. Evans, V. Stezov, and T. J. Evans, Assessment of utility energy storage options for increased renewable energy penetration, *Renewable and Sustainable Energy Reviews* **2012**, 16, 4141 – 4147.
2. M. Lazzari and B. Scrosati, A cyclable lithium organic electrolyte cell based on two intercalation electrodes, *J. Electrochem. Soc.* **1980**, 127, 773 – 774.
3. N. Nitta, F. Wu, J. T. Lee, G. Yushin, Li-ion battery materials: present and future *Materials Today*, **2015**, 18, 252 – 264.
4. K. Mizushima, P. C. Jones, P. J. Wiseman, J. B. Goodenough, $LixCoO_2$ ($0 < x < -1$): A new cathode material for batteries of high energy density, *Mater. Res. Bull.* **1980**, 15, 783 – 789.

5. K. Ozawa, Lithium-ion rechargeable batteries with $LiCoO_2$ and carbon electrodes: the $LiCoO_2$/C system, *Solid State Ionics*, **1994**, 69, 212-221.
6. J. M. Paulsen, J. R. Muller-Neuhaus, and J. R. Dahn, Layered $LiCoO_2$ with a different oxygen stacking (O_2 structure) as a cathode material for rechargeable lithium batteries, J. Electrochem. Soc., **2000**, 147, 508 – 516.
7. J. P. Peres, F. Weill, C. Delmas, Lithium/vacancy ordering in the monoclinic LixNiO2 ($0.50 \leq x \leq 0.75$) solid solution, *Solid State Ionics*. **1999**, 116, 19 – 27.
8. T. Ohzuku, Y. Makimura, Layered lithium insertion material of $LiCo_{1/3}Ni_{1/3}Mn_{1/3}O_2$ for lithium-ion batteries, Chem. Lett. **2001**, 30, 642–643.
9. Z. L. Gong and Y. Yang, Recent advances in the research of polyanion-type cathode materials for Li-ion batteries. *Energy & Environ. Sci*. **2011**, 4, 3223 – 3242.
10. E. Rossen, J. N. Reimers, J. R. Dahn, Synthesis and electrochemistry of spinel LT $LiCoO_2$, Solid State Ionics, **1993**, 62, 53-60.
11. B. Garcia, J. Farcy, J. P. Pereira-Ramos, J. Perichon, N. Baffier, Low-temperature cobalt oxide as rechargeable cathodic material for lithium batteries, *J. Power Sour.* **1995**, 54, 373 – 377.
12. R. J. Gummow, M. M. Thackeray, W. I. F. David, S. Hull, Structure and electrochemistry of lithium cobalt oxide synthesized at 400ºC, *Mater. Res. Bull.* **1992**, 27, 327 – 337.
13. E. Zhecheva, R. Stoyanova, M. Gorova, R. Alcantara, J. Morales, J. L. Tirado, Lithium-cobalt precursors in the preparation of intercalation electrode materials, *Chem. Mater*. **1996**, 8, 1429 – 1440.
14. E.-D. Jeong, M.-S. Won, and Y.-B. Shim, Cathodic properties of a lithium-ion secondary battery using $LiCoO_2$ prepared by a complex formation reaction, *J. Power Sour.* **1998**, 70, 70 – 77.
15. Y. Li, C. Wan, Y. Wu, C. Jiang, and Y. Zhu, Synthesis and characterization of ultrafine $LiCoO_2$ powders by a spray drying method, *J. Power Sour.* **2000**, 85, 294 – 298.
16. P. N. Kumta, D. Gallet, A. Waghray, G. E. Bomgren, and M. P. Setter, Synthesis of $LiCoO_2$ powders for lithium-ion batteries from precursors derived by rotary evaporation, *J. Power Sour.* **1998**, 72, 91 - 98.

 doi:10.20944/preprints201808.0046.v1

17. W. Li, S. Zhang, and J. Chen, Synthesis, characterization, and electrochemical application of $Ca(OH)_2$, $Co(OH)_2$, and $Y(OH)_3$ – coated $Ni(OH)_2$ tubes, *J. Phys. Chem B*. **2005**, 109, 14025 – 14032.

18. W. Cao, and W. Wang, Three-dimensional flower-like α-$Co(OH)_2$ architectures assembled by nanoplates for lithium ion batteries, *Mater. Lett*. **2016**, 185, 495 – 498.

19. P. S. Gaikar, S. T. Navale, S. L. Gaikwad, A. Al-Osta, V. V. Jadhav, P. R. Arjunwadkar, M. Naushad, and R. S. Mane, Pseudocapacitive performance of a solution-processed β-$Co(OH)_2$ electrode monitored through its surface morphology and area, *Dalton Trans.* **2017**, 46, 3393 – 3399.

20. M. Aghazadehn, S. Dalvand, M. Hosseinifard, Facile electrochemical synthesis of uniform β-$Co(OH)_2$ nanoplates for high performance supercapacitors, *Ceramics International*, **2014**, *40*, 3485 – 3493.

21. B. Wang, H. Lin, Z. Yin, Hydrothermal synthesis of β-cobalt hydroxide with various morphologies in water / ethanol solutions, *Materials Letters*, **2011**, 65, 41 - 43.

22. J. Yang, H. Lu, W. N. Martens, and R. L. Frost, Synthesis and characterization of cobalt hydroxide, cobalt oxyhydroxide, and cobalt oxide nanodiscs, *J. Phys. Chem. C*. **2010**, 114, 111 – 119.

23. P. Hartman, Structural morphology of organic compounds having two centrosymmetric molecules in a monoclinic unit cell, *J. Crystal Growth*, **1991**, 110, 559 -570.

24. J. Hong, N. Matsushita, T. Shirai, K. Nakata, C. terashima, A. Fujishima, and K. Katsumata, Influence of surface morphology and conductivity on photocatalytic performance of solution-processed zinc oxide film, *Chem. Asian J*. **2017**, 12, 2480 – 2485.

25. V. Pralong, A. Delahaye-Vidal, B. Beudoin, B. Gerand, and J.-M. Tarascon, Oxidation mechanism of cobalt hydroxide to cobalt oxyhydroxide, *J. Mater. Chem*. **1999**, 9, 955 – 960.

26. Z. P. Xu, and H. C. Zeng, Interconversion of brucite-like and hydrotalcite-like phases in cobalt hydroxide compounds, *Chem. Mater*. **1999**, 11, 67 – 74.

Preprints (www.preprints.org) | NOT PEER-REVIEWED | Posted: 2 August 2018 doi:10.20944/preprints201808.0046.v1

Table of Content (ToC)

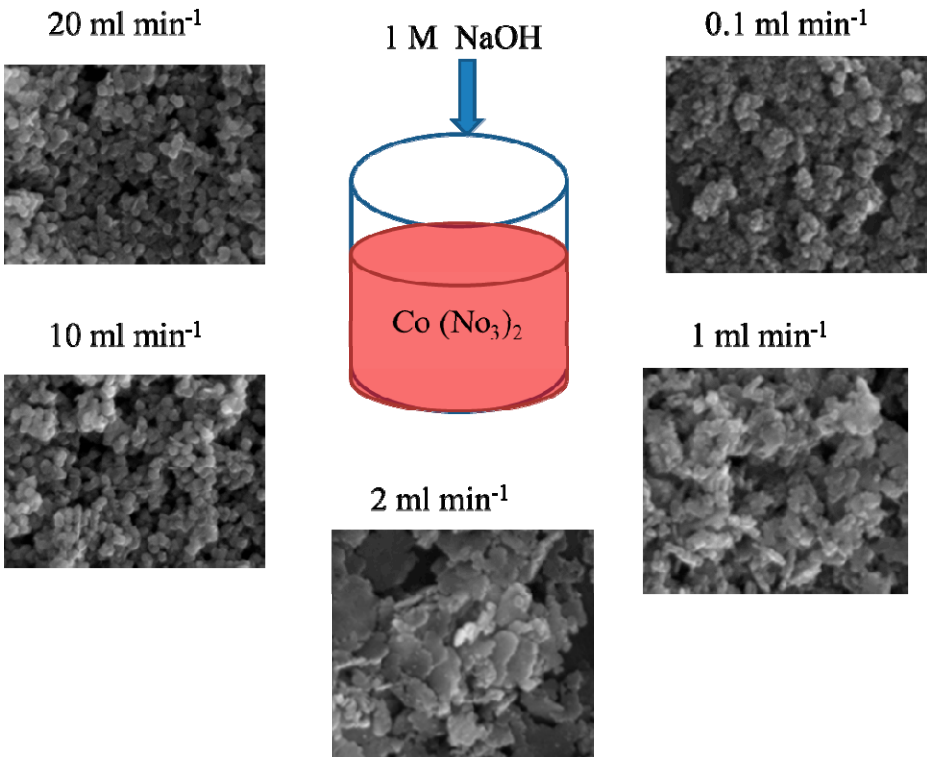

"Crystalline β-cobalt hydroxide of different morphologies have been successfully synthesized with the addition of sodium hydroxide to cobalt nitrate solution and ageing in mother liquor then used as a precursor to prepare battery electrode $LiCoO_2$."

Preprints (www.preprints.org) | NOT PEER-REVIEWED | Posted: 2 August 2018 doi:10.20944/preprints201808.0046.v1

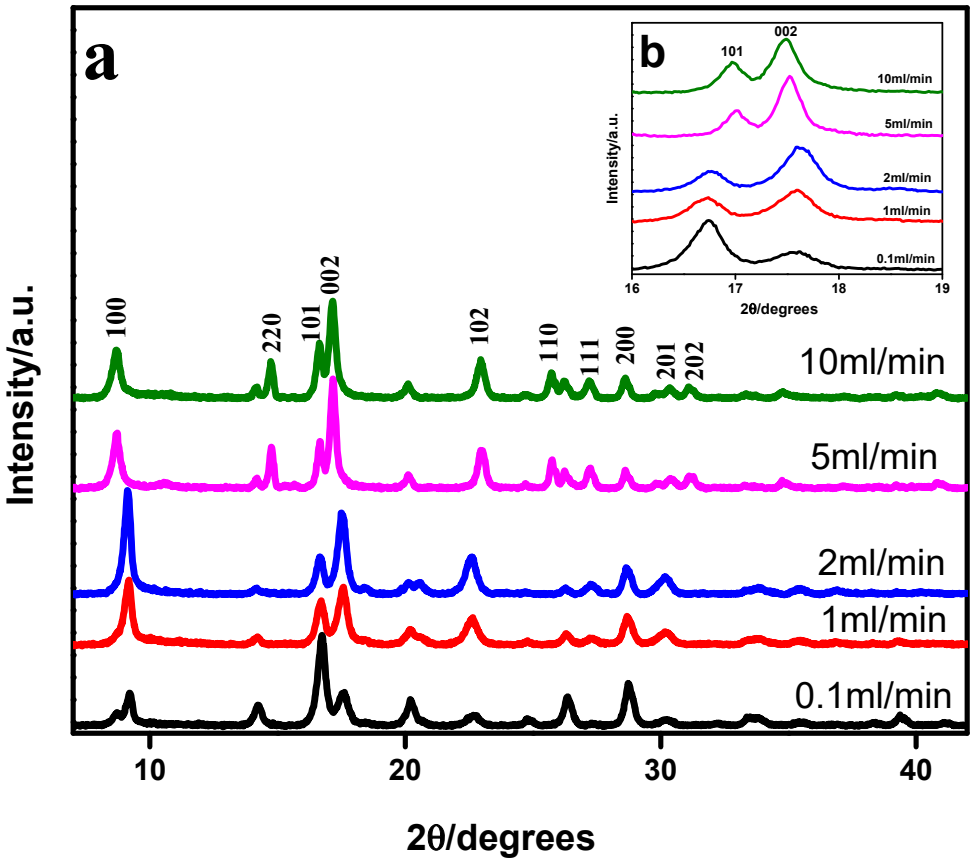

Figure 1 (a) X-ray diffraction (XRD) patterns of the as-synthesized β-$Co(OH)_2$ in the presence of NaOH addition at a different rate indicated in the figure, and (b) magnified XRD pattern of the 2θ values between 16º and 19º. Variation in the intensity of the doublet peaks (101) and (002) shown in the inset.

Preprints (www.preprints.org) | NOT PEER-REVIEWED | Posted: 2 August 2018 doi:10.20944/preprints201808.0046.v1

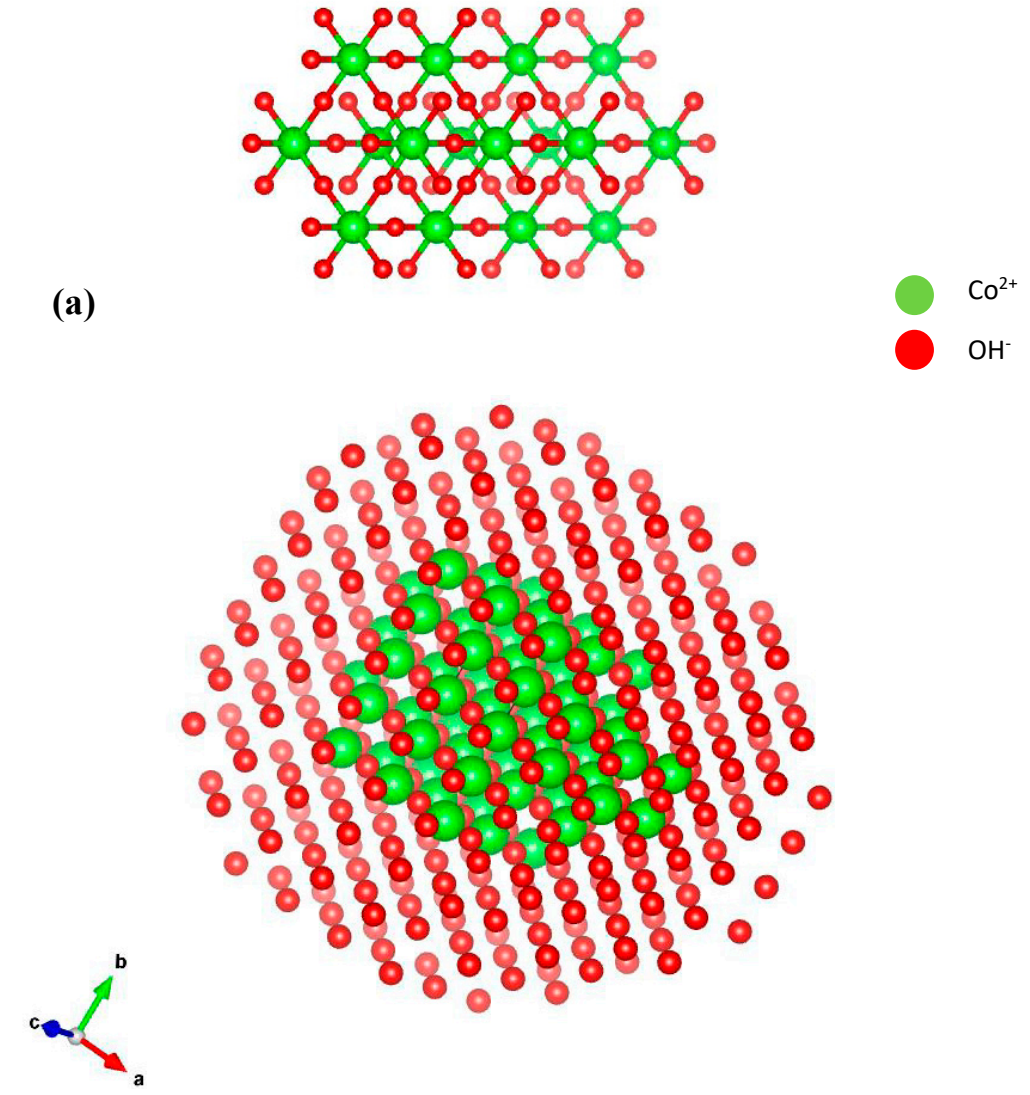

Figure 2 Ball and stick diagram of the formation of β-$Co(OH)_2$ in the presence of (a) optimised amount and (b) excess amount of OH^- ions in the solution. Picture (b) is viewed in (002) plane.

Preprints (www.preprints.org) | NOT PEER-REVIEWED | Posted: 2 August 2018 doi:10.20944/preprints201808.0046.v1

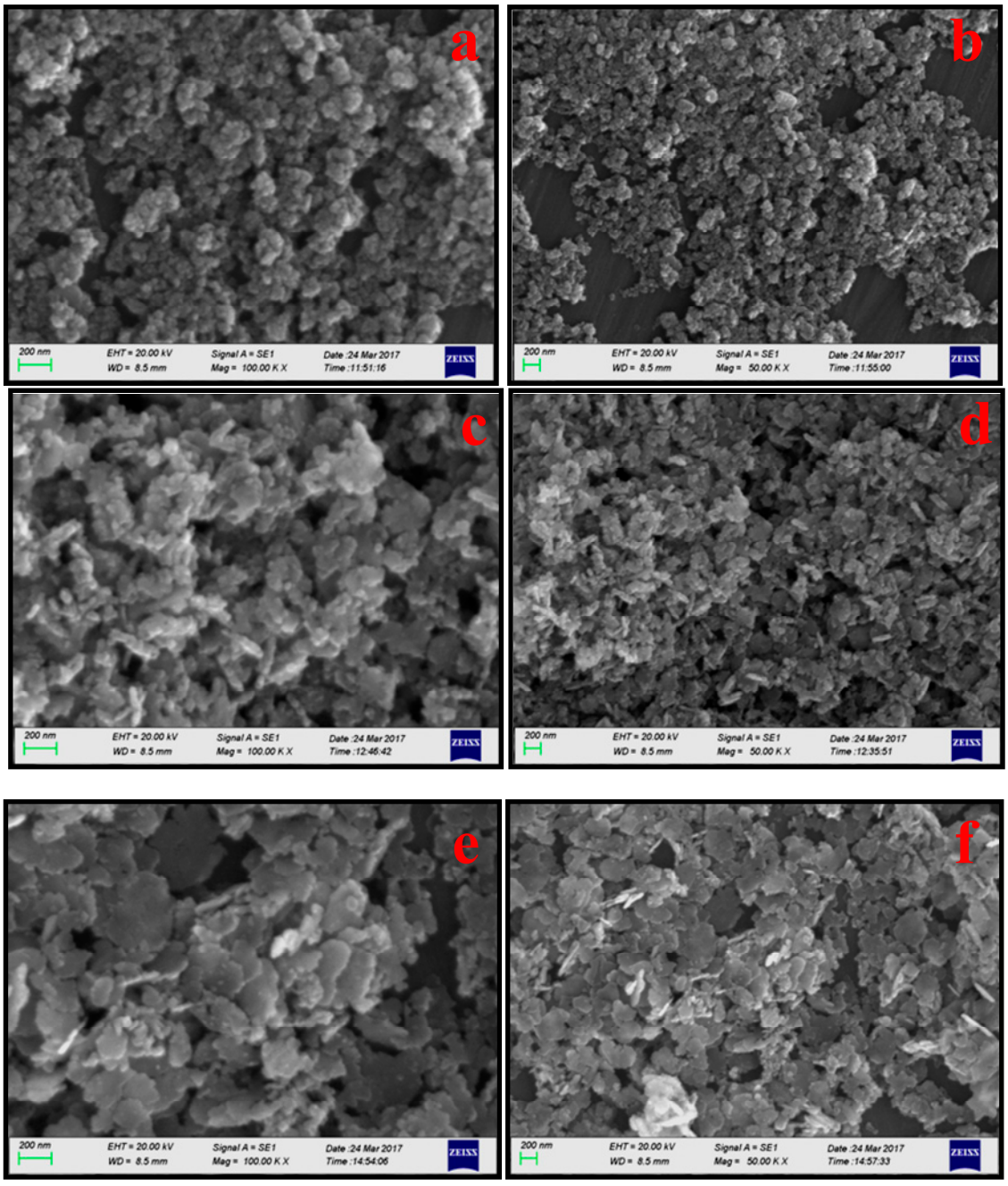

Preprints (www.preprints.org) | NOT PEER-REVIEWED | Posted: 2 August 2018 doi:10.20944/preprints201808.0046.v1

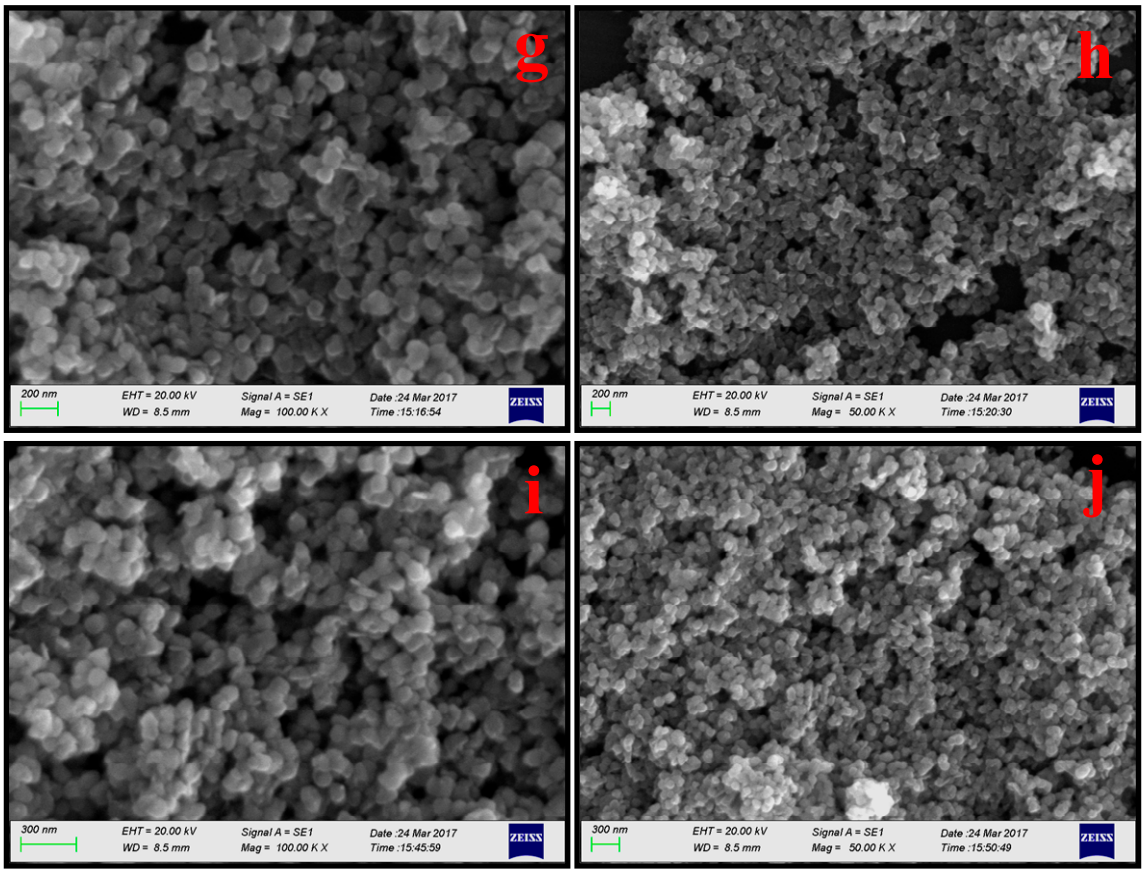

Figure 3 Scanning electron micrographs (SEM) of as-synthesized β-$Co(OH)_2$ in the presence of NaOH addition at a different rate **(a, b)** 0.1 mL/min **(c, d)** 1 mL/min **(e, f)** 2 mL/min **(g ,h)** 5 mL/min **(i, j)**10 mL/min on different magnifications. Change in morphology is evident. Platelets like shape (c – f), and tiny clusters (g – j).

Preprints (www.preprints.org) | NOT PEER-REVIEWED | Posted: 2 August 2018 doi:10.20944/preprints201808.0046.v1

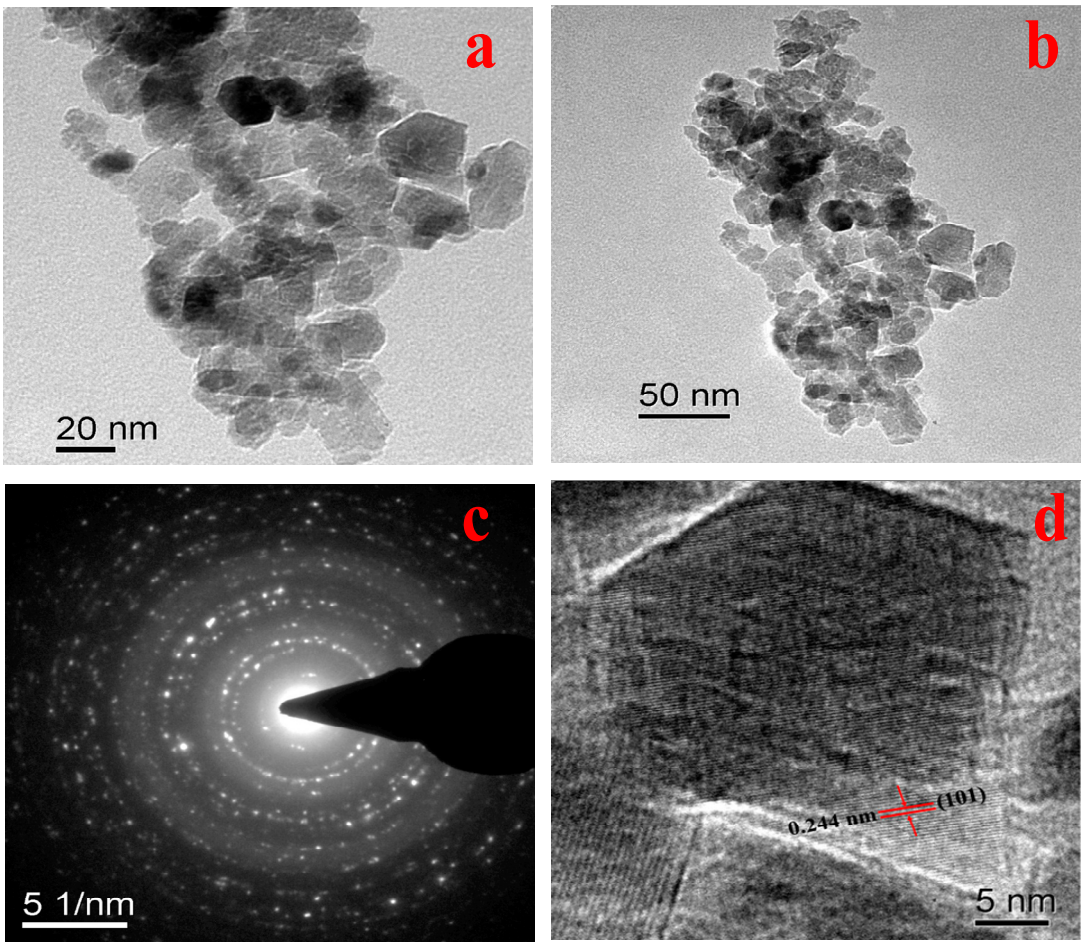

Figure 4 Transmission electron micrographs (TEM) of as-synthesized β-$Co(OH)_2$ in the presence of NaOH addition at a 0.1 mL/min rate. (a-b) showing hexagonal shaped particles under different magnifications, (c) its corresponding selected area diffraction pattern (SADP) and (d) high resolution TEM (HRTEM) showing fringes like pattern, interplanar distance between two fringes is shown.

Preprints (www.preprints.org) | NOT PEER-REVIEWED | Posted: 2 August 2018 doi:10.20944/preprints201808.0046.v1

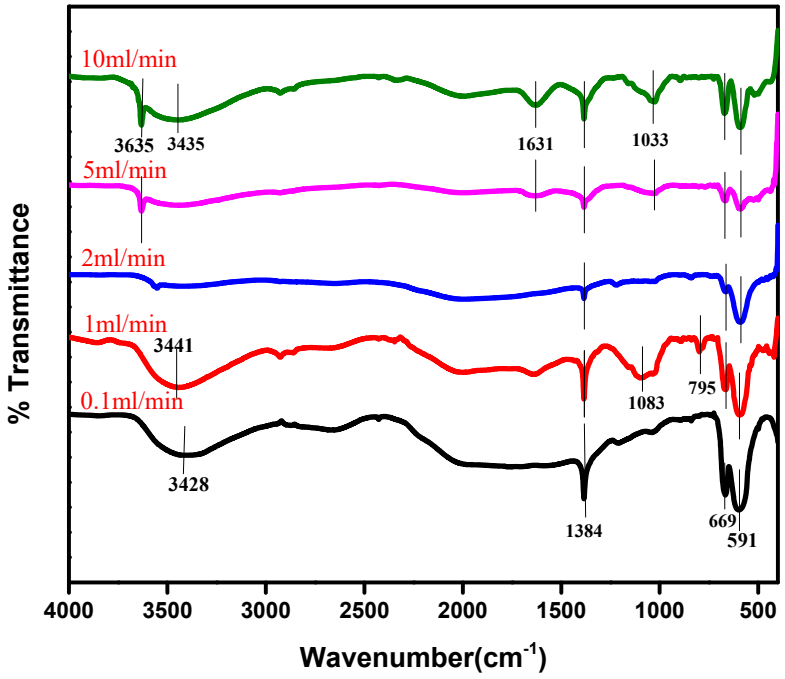

Figure 5 Fourier transform infra-red spectra of the as-synthesized β-$Co(OH)_2$ in the presence of NaOH addition at a different rate indicated in the figure.

Preprints (www.preprints.org) | NOT PEER-REVIEWED | Posted: 2 August 2018 doi:10.20944/preprints201808.0046.v1

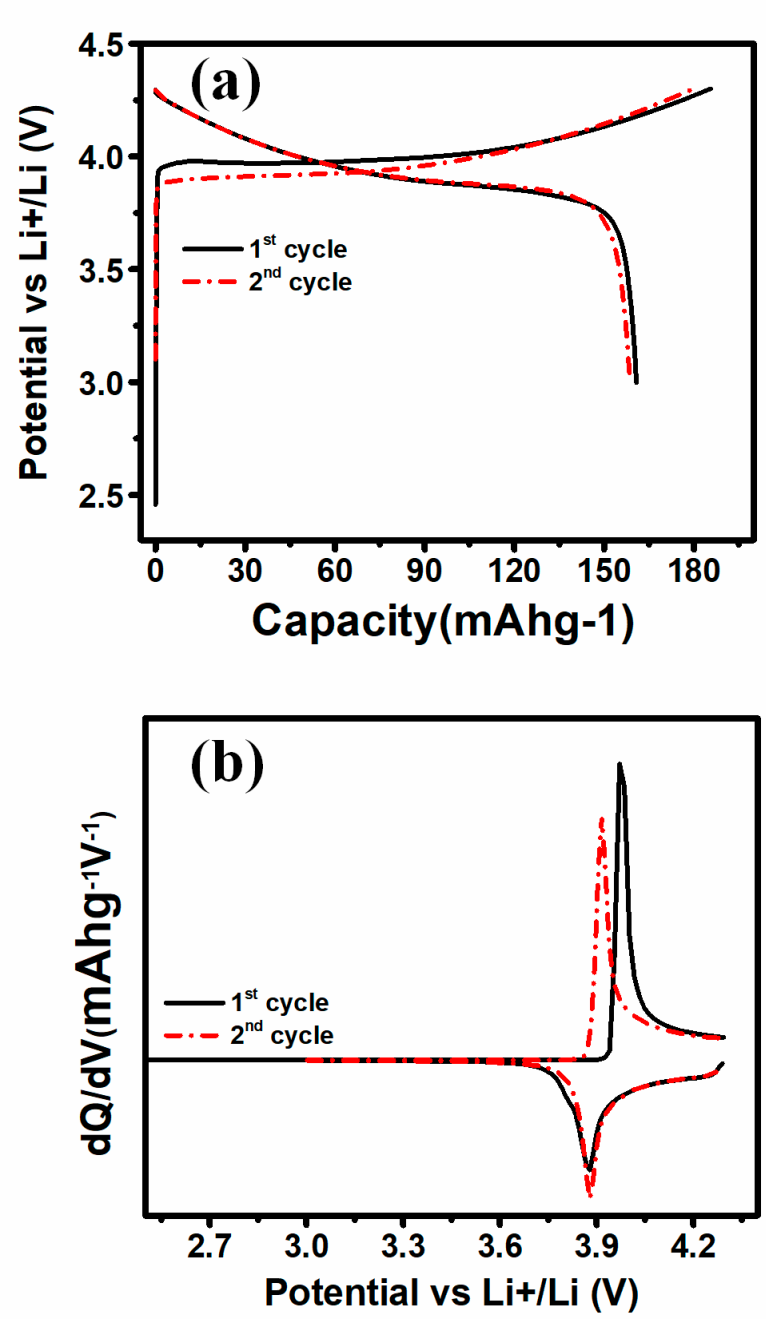

Figure 6 (a) Charge – discharge profile of as-synthesized β-$Co(OH)_2$ in the presence of NaOH addition at a 0.1 mL/min rate illustrating the cell is fully reversible after subsequeent cycles, and (b) corresponding dQ/dV plot.

Preprints (www.preprints.org) | NOT PEER-REVIEWED | Posted: 2 August 2018 doi:10.20944/preprints201808.0046.v1

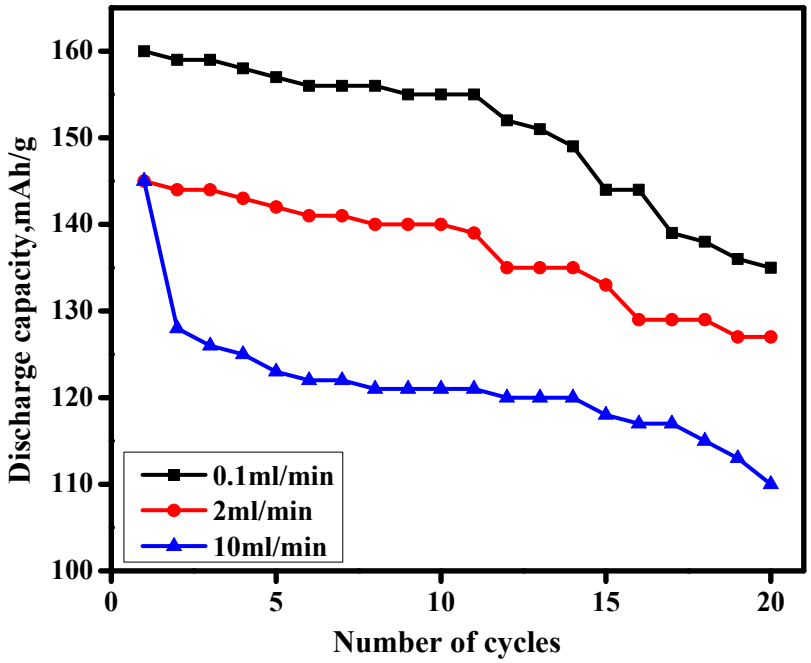

Figure 7 Discharge capacity upon cycling illustrating the cycling stability of the as-synthesized β-$Co(OH)_2$ in the presence of NaOH addition at a different rate indicated in the figure. The lower rate provides us a larger discharge capacity and excellent cycling stability.

Preprints (www.preprints.org) | NOT PEER-REVIEWED | Posted: 2 August 2018 doi:10.20944/preprints201808.0046.v1

Table 1 Particle size analysis of the as-synthesized β-$Co(OH)_2$

Rate (mL/min)	Size (nm)	
	50%	**90%**
0.1	237.1	290.7
1	420.0	901.0
2	525.0	2939
5	232.9	973.0
10	402.0	539.0

Table 2 Performance characteristics of the as-synthesized β-$Co(OH)_2$ in the presence of NaOH addition at a different rate indicated in the figure. Capacity retention and rate of discharge are compared.

Discharge rate	Rate of addition (mL/ min)	Initial discharge capacity(mAh/g)	Average discharge capacity (mAh/g)	Average fading rate (mAh/g per cycle)
C/20	0.1	135	151.5	1.26
C/5		156	158.6	0.6
C/2		159	159.5	0.5
C/20	2	127	137.4	0.94
C/5		141	143.6	0.6
C/2		144	144.5	0.5
C/20	10	110	121.8	1.68
C/5		122	129.4	4.4
C/2		128	136.5	8.5